Simulation of an 1857-like Mw 7.9 San Andreas fault earthquake and the response of tall steel moment frame buildings in southern California - A prototype study

S. Krishnan[1], C. Ji[2], D. Komatitsch[3], J. Tromp[4], M. Muto[5], J. Mitrani-Reiser[6], J. L. Beck[7]

[1] *Asst. Professor, Dept. of Civil Engineering, California Institute of Technology, Pasadena, USA*
Email: krishnan@caltech.edu

[2] *Asst. Professor, Dept. of Earth Science, University of California, Santa Barbara, USA*

[3] *Professor, Dept. of Modeling and Imaging in Geosciences, University of Pau, France*

[4] *Professor, Geosciences and Applied & Computational Mathematics, Princeton University, Princeton, USA*

[5] *Post-Doctoral Scholar, Dept. of Civil Engineering, California Institute of Technology, Pasadena, USA*

[6] *Asst. Research Professor, Dept. of Civil Engineering, Johns Hopkins University, Baltimore, USA*

[7] *Professor, Dept. of Civil Engineering, California Institute of Technology, Pasadena, USA*

ABSTRACT :

In 1857, an earthquake of magnitude 7.9 occurred on the San Andreas fault, starting at Parkfield and rupturing in a southeasterly direction for more than 360 km. Such a unilateral rupture produces significant directivity toward the San Fernando and Los Angeles basins. The strong shaking in the basins due to this earthquake would have had significant long-period content (2-8 s), and the objective of this study is to quantify the impact of such an earthquake on two 18-story steel moment frame building models, hypothetically located at 636 sites on a 3.5 km grid in southern California. End-to-end simulations include modeling the source and rupture of a fault at one end, numerically propagating the seismic waves through the earth structure, simulating the damage to engineered structures and estimating the economic impact at the other end using high-performance computing. In this prototype study, we use an inferred finite source model of the magnitude 7.9, 2002 Denali fault earthquake in Alaska, and map it onto the San Andreas fault with the rupture originating at Parkfield and propagating southward over a distance of 290 km. Using the spectral element seismic wave propagation code, SPECFEM3D, we simulate an 1857-like earthquake on the San Andreas fault and compute ground motions at the 636 analysis sites. Using the nonlinear structural analysis program, FRAME3D, we subsequently analyze 3-D structural models of an existing tall steel building designed using the 1982 Uniform Building Code (UBC), as well as one designed according to the 1997 UBC, subjected to the computed ground motion at each of these sites. We summarize the performance of these structural models on contour maps of peak interstory drift. We then perform an economic loss analysis for the two buildings at each site, using the Matlab Damage and Loss Analysis (MDLA) toolbox developed to implement the PEER loss-estimation methodology. The toolbox includes damage prediction and repair cost estimation for structural and non-structural components and allows for the computation of the mean and variance of building repair costs conditional on engineering demand parameters (i.e. inter-story drift ratios and peak floor accelerations). Here, we modify it to treat steel-frame high-rises, including aspects such as mechanical, electrical and plumbing systems, traction elevators, and the possibility of irreparable structural damage. We then generate contour plots of conditional mean losses for the San Fernando and the Los Angeles basins for the pre-Northridge and modern code-designed buildings, allowing for comparison of the economic effects of the updated code for the scenario event. In principle, by simulating multiple seismic events, consistent with the probabilistic seismic hazard for a building site, the same basic approach could be used to quantify the uncertain losses from future earthquakes.

KEYWORDS:
End-to-end simulation; seismic wave propagation; nonlinear analysis; tall steel moment frame buildings; high performance computing in earthquake engineering; economic loss analysis.

1. INTRODUCTION

The risk of earthquakes in southern California arises from two sources: well mapped-out faults such as the San Andreas, Newport-Inglewood, and Santa Monica-Hollywood-Raymond faults that have some form of surface

expression, and the network of blind-thrust faults hidden deep inside the Earth that includes the Northridge fault and the Puente Hills fault underneath downtown Los Angeles. While the blind-thrust faults have the potential for rare (recurrence intervals of 1000-3000 years) and moderate magnitude ~7 earthquakes (Shaw and Suppe, 1996), large magnitude 7.5-8.0 earthquakes have been occurring fairly regularly (every 140--300 years) on the San Andreas strike-slip fault system (Sieh 1977, 1978, Weldon et al. 2005). As a result of their frequent recurrence, it is the San Andreas fault events that arguably govern the risk posed to tall buildings in southern California. Fortunately, in modern history the urban areas of southern California have thus far been spared from the strongest shaking generated by large strike-slip earthquakes on the San Andreas fault, with the last major earthquake (magnitude 7.9) occurring in 1857, when the population of southern California was about 25,000. In that event rupture initiated at Parkfield in central California, and propagated in a southeasterly direction a distance of 360 km. Such a unilateral rupture produces significant directivity toward the San Fernando and Los Angeles basins. Indeed, newspaper reports of sloshing observed in the Los Angeles river point to long-duration (1-2 min) and long-period (2-8 s) shaking, which would preferentially excite tall structures in the two basins.

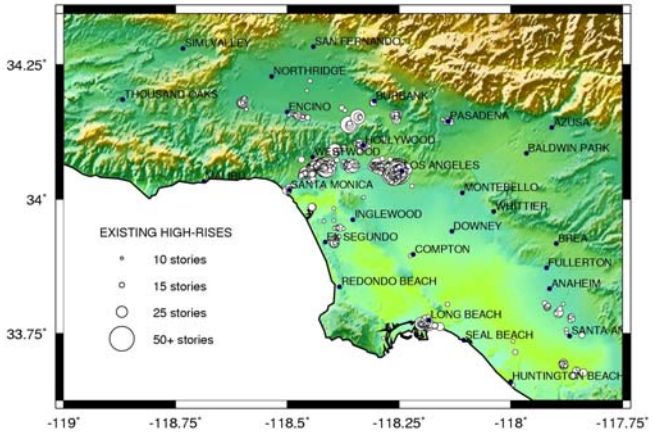

Figure 1: Distribution of tall buildings (10 stories or greater) in the Los Angeles metropolitan area as of mid-2007. There are 489 buildings with 10-19 stories, 118 buildings with 20-29 stories, 28 buildings with 30-39 stories, 11 buildings with 40-49 stories, and 10 buildings with 50 or more stories. Data source: Emporis.com by way of Keith Porter, University of Colorado at Boulder.

The location of tall buildings in the Los Angeles metropolitan area with 10 or more stories is shown in Figure 1. The buildings are clustered in small pockets that are aligned with the major freeways in the region. Most tall buildings have been built along Interstate freeway I-10 from Santa Monica to downtown Los Angeles, in the mid-Wilshire district along Wilshire boulevard, and along State Highway 101 from Hollywood to Canoga Park in the San Fernando valley. In addition, a few tall buildings are located along Interstate freeways, I-5 and I-405. The 14 locations where highrise buildings are concentrated are Canoga Park, Encino, Santa Monica, Century City, Universal City, Park La Brea, Hollywood, Glendale, El Segundo, downtown Los Angeles, Pasadena, Long Beach, Santa Ana-Anaheim corridor, and Irvine. There are a few solitary towers scattered across the region, but for the purposes of region-wide hazard assessment, close attention may be paid to these 14 tall building clusters. The size of circles shown in the figure is proportional to the number of stories. There are 489 buildings with 10-19 stories, 118 buildings with 20-29 stories, 28 buildings with 30-39 stories, 11 buildings with 40-49 stories, and 10 buildings with 50 or more stories. Many more are in the planning stages or under construction. It is clear that majority (607) are in the 10-30 story range. Typical lateral force-resisting systems for structures in this height range are steel moment frames, steel braced frames, concrete moment frames, and concrete shear wall systems. In the 25-30 story range, dual systems comprising of a combination of perimeter steel moment frames and braced frame core, or perimeter concrete moment frames and shear wall core may have been utilized. Nevertheless, we could assume that about one-quarter of the 607 buildings in the

10-29 story range utilize steel moment frames as their primary lateral force resisting system

The magnitude 6.7 earthquake of January 17, 1994, on the Northridge blind-thrust fault caused 57 deaths and economic losses in excess of $40 billion (Eguchi et al. 1998, Petak and Elahi 2000). This earthquake exposed the vulnerability of steel moment-resisting frame buildings to fracture (SAC 1995a, 1995b, 1995c). These buildings resist lateral forces from an earthquake through bending in rigidly-connected (welded) beams and columns. However, due to certain construction practices and the use of non-ductile weld material, a significant number of connections fractured in some of these buildings. Many of the moment-frame buildings in southern California were constructed before 1976 (EQE 1995a), when there was inadequate understanding of the nature and power of earthquake forces and their effects on buildings. Therefore, the question arises as to what would happen to the many tall steel buildings in the Los Angeles and San Fernando basins if the 1857 San Andreas fault earthquake were to occur today. Can we estimate damage and consequent losses in these buildings? There have been many improvements in building codes and construction practices since 1994, and buildings designed according to current codes, termed ``new/redesigned buildings'' in this article, are expected to perform far better than existing buildings, defined as those designed using codes preceding the 1997 Uniform Building Code (UBC97), in large earthquakes. Will they in fact, and, if so, is this performance adequate? Before we can answer these questions, we need to be able to answer more fundamental questions, e.g.: what kind of shaking would be experienced in this region during such an earthquake? What would the frequency content of the shaking be? What about the amplitude and duration of significant shaking? We have a qualitative feel for the extent and intensity of ground shaking from newspaper reports (Agnew and Sieh 1978, Meltzner and Wald 1998) following the magnitude 7.9 San Andreas fault earthquake of January 9, 1857. However, we need estimates of the ground motion waveforms for performing quantitative seismic hazard assessment in a rigorous manner.

In this study we combine state-of-the-art computational tools in seismology, structural engineering, and economic loss analysis to perform a three-dimensional (3-D) end-to-end simulation of the rupture of a 290 km section of the San Andreas fault, the generation and propagation of the resulting seismic waves, the subsequent ground shaking in the Los Angeles and San Fernando basins, the resulting damage and mean loss to two 18-story steel moment-frame buildings in the entire region. Each of these parts requires simulation at very different temporal and spatial scales that are best performed using task-specific software.

2. 1857-LIKE SAN ANDREAS FAULT EARTHQUAKE: GROUND MOTION SIMULATION (Krishnan et al. 2006a)

The seismological domain of our analysis includes all of southern California and extends north into the central valley beyond Parkfield. However, we restricted the engineering analysis to the main sedimentary basins of San Fernando, Los Angeles, and San Gabriel (Figure 2). For the 1857 scenario, ground motions south of Irvine going towards San Diego are unlikely to be strong enough to warrant a detailed engineering analysis. The solid circles in the figure denote some of the major cities in the region. We have divided the region using a grid spaced at 1/32 of a degree (i.e., about 3.5km) each way. There is a total of 636 sites. Also shown in the figure is the surface projection of the Northridge fault that ruptured during the January 17, 1994 earthquake. The inset illustrates the region of interest in relation to the San Andreas fault rupture scenarios under consideration. We take a deterministic approach to simulate ground motion based upon the spectral-element method (e.g., Komatitsch and Tromp 1999). The numerical simulations, which account for 3-D variations of seismic wave speeds (Harvard-LA velocity model, Suss and Shaw 2003) and density, topography and bathymetry, and attenuation, are carried out using our open-source seismic wave propagation package SPECFEM3D (http://www.geodynamics.org). The methodology adopted therein has been shown to reliably model ground motion down to a period of approximately 2s using data from recent earthquakes (Komatitsch et al. 2004, Liu et al. 2004).

2.1.Source Model

For a San Andreas simulation it is critical to have a realistic source model (slip distribution as a function of time

along the fault). On November 3, 2002, a magnitude 7.9 earthquake occurred on the vertical, right-lateral, Denali strike-slip fault system in Alaska, which is geometrically similar to the San Andreas fault. For the simulation of the 1857-like San Andreas earthquake, the slip on the Denali fault system during the 2002 earthquake is mapped onto the San Andreas fault, with the rupture initiating at Parkfield and progressing in a southeasterly direction over a distance of about 290km (Figure 3). The maximum depth of rupture is about 20km. The surface slip grows slowly to 7.4m and drops off drastically towards the end of the rupture. The peak slip at depth is about 12m.

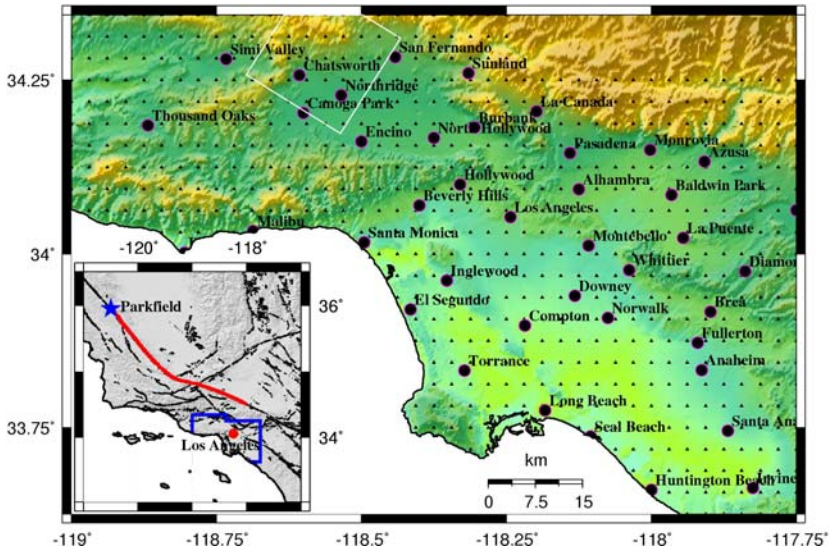

Figure 2: Geographical scope of the San Andreas fault earthquake simulation. The color scheme reflects topography, with green denoting low elevation and yellow denoting mountains. The solid black triangles represent the 636 sites at which seismograms are computed and buildings are analyzed. The white box is the surface projection of the Northridge fault. The red line in the inset is the surface trace of the hypothetical 290 km rupture of the San Andreas fault that is the primary focus of this study. The area enclosed by the blue polygon denotes the region covered by the 636 sites.

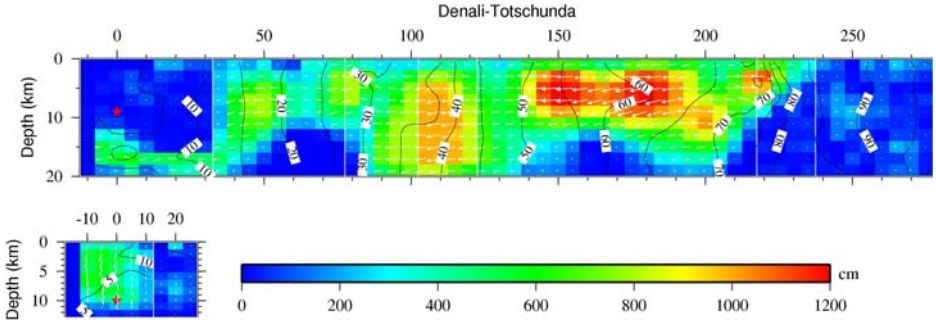

Figure 3: Slip distribution of the November 3, 2002, magnitude 7.9 Denali, Alaska, earthquake constrained by teleseismic body and strong motion waveforms as well as GPS vectors. The color scheme reflects the slip amplitude and contours reflect the rupture initiation time. The hypocenter is indicated by the red star. White arrows denote the slip direction and magnitude. Numbers in white squares denote the rupture times in seconds.

2.2. Peak Ground Motion

Using the spectral-element method, we compute seismograms at each of the 636 hypothetical tall-building sites (Figure 2). The minimum S wave velocity in the Harvard-LA basin model is 687m.s^{-1}. The horizontal size of the mesh cells at the surface is approximately 270m in each direction. The resulting number of grid points per

S wavelength is about 5. The time step used for the computations is 9ms, with a total number of 30000 steps, i.e., a total duration of 270s. Shown in Figure 4 are maps of peak velocity and displacement of the three components of ground motion, lowpass-filtered at a corner period of 2s. The San Fernando valley experiences severe shaking. As the rupture proceeds down south from Parkfield and hits the bend in the San Andreas fault, it sheds off a significant amount of energy into the region that is directly in front of it, which happens to be the San Fernando valley (see http://krishnan.caltech.edu for a movie of the rupture and seismic wave propagation). A good portion of this energy spills over into the Los Angeles basin, with many cities along the coast, such as Santa Monica and Seal Beach, and more inland areas, going east from Seal beach towards Anaheim, experiencing long-duration shaking. In addition, the tail-end of the rupture sheds energy from SH/Love waves into the Baldwin Park-La Puente region, which is bounded by a line of mountains that creates a mini-basin, further amplifying the ground motion. The peak velocity is of the order of $1 m.s^{-1}$ in the Los Angeles basin, including downtown Los Angeles, and $2 m.s^{-1}$ in the San Fernando valley. The map of peak displacements has characteristics quite similar to that of the peak velocities, with significant displacements in the basins but not in the mountains. The peak displacements are in the neighborhood of 1m in the Los Angeles basin and 2m in the San Fernando valley.

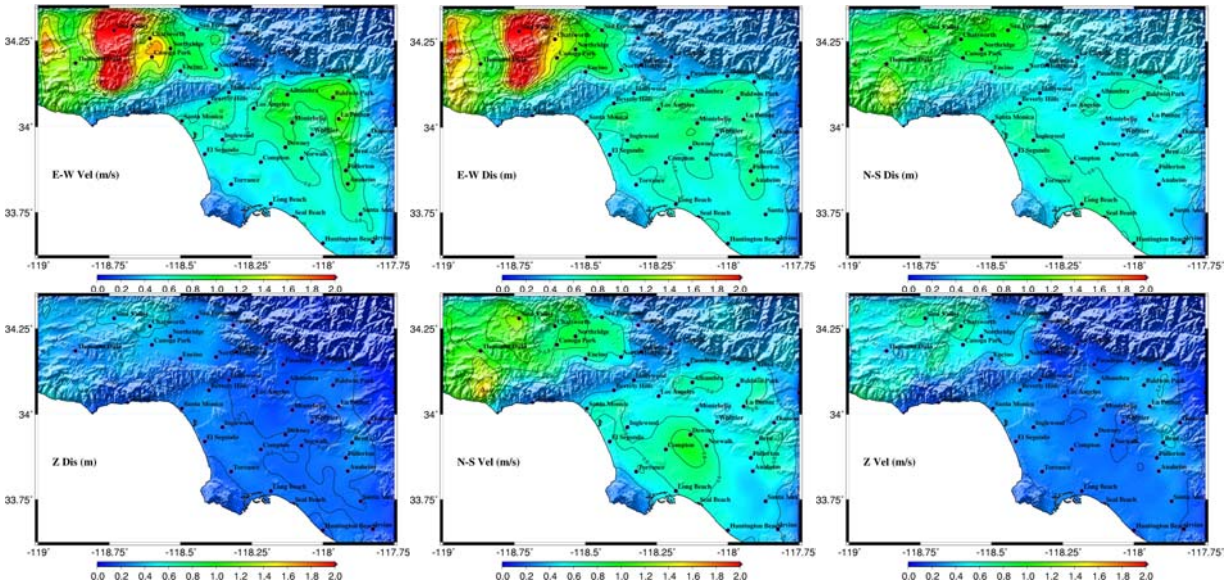

Figure 4: East-west, north-south, and vertical components of the peak ground velocities and displacements of the synthetic seismograms lowpass-filtered with a corner period of 2s from the 1857-like San Andreas fault earthquake simulation.

3. BUILDING DAMAGE ANALYSIS (Krishnan et al. 2006b)

3.1. Buildings Considered

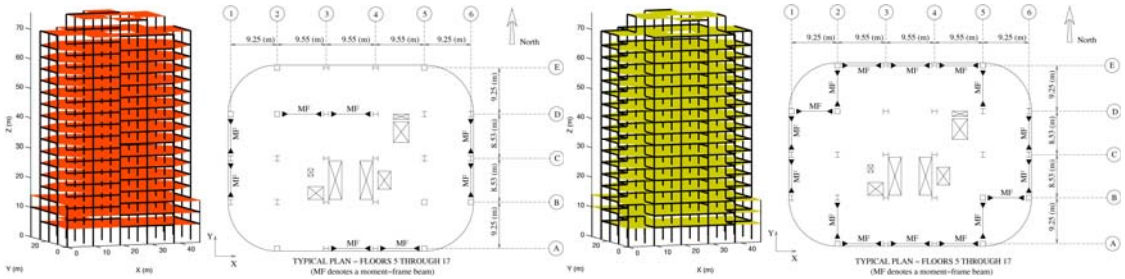

Figure 5: FRAME3D models of two steel moment frame buildings – an existing building designed using the 1982 UBC and a redesigned building designed using the 1997 UBC, and typical plan views showing the

location of columns and moment-frame beams. Note the greater number of moment-frame bays in the redesigned building.

The impact of the 1857-like San Andreas fault earthquake on two 75.7m high, 18-story steel moment frame buildings – one existing and one hypothetical - is investigated. The existing building, located on Canoga Avenue in Woodland Hills, was designed using the 1982 UBC. It suffered significant damage (fracture in moment connections) during the 1994 Northridge earthquake and has been the subject of detailed study by many research groups following the Northridge earthquake (SAC 1995b). The second building is similar to the base building, but the structural system (lateral force-resisting system) has been redesigned according to UBC97. The 1997 code regulations specify larger design forces (to account for near-source effects) and call for greater redundancy in the lateral force-resisting system. This results in a greater number of bays of moment frames. The fundamental natural period of the existing building is 4.43s, whereas that of the redesigned building is 3.72s. Two other distinguishing factors of the existing building are torsional eccentricity and moment connections that are susceptible to fracture.

3.2. Building Response

3-D models of the two buildings are analyzed for the simulated three-component ground motion waveforms at each of the 636 analysis sites using the nonlinear structural analysis program, FRAME3D (Krishnan and Hall 2006a, 2006b). Material nonlinearity resulting in flexural yielding, strain-hardening, and ultimately rupturing of steel at the ends of beams and columns, and shear yielding in panel-zones is included. The program includes a geometry updating feature to accommodate large translations and rotations, automatically accounting for P-Δ effects and allowing the analysis to follow a structure's response well into collapse. Brittle failure of moment connections due to fracture is included. However, local flange buckling in beams and columns is not. Column splices are not modeled either.

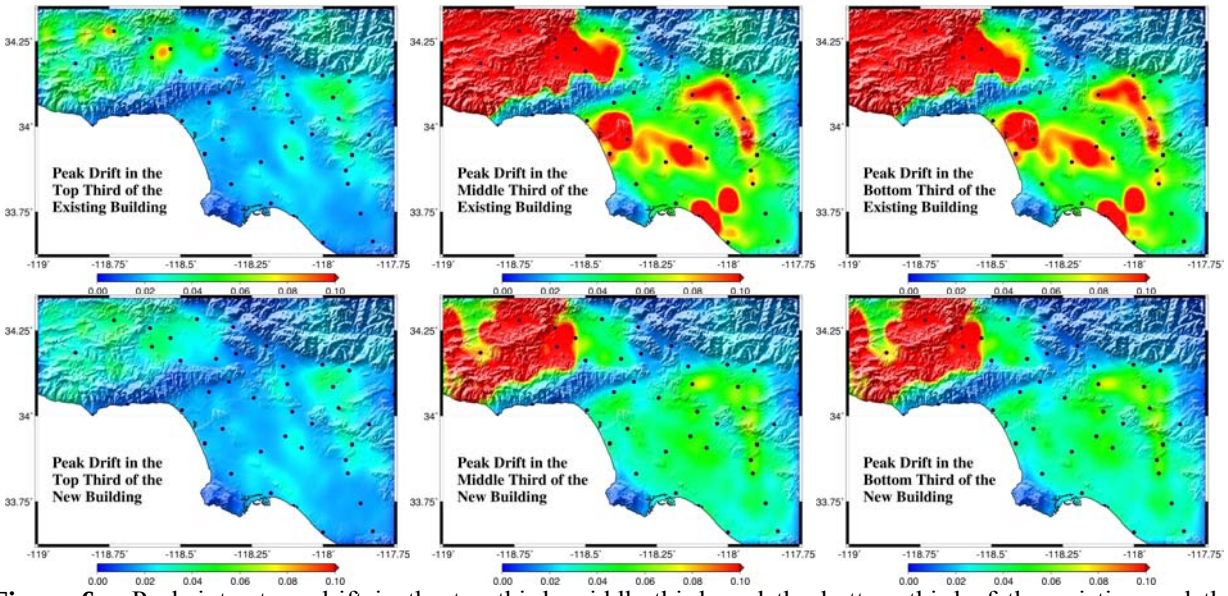

Figure 6: Peak interstory drift in the top-third, middle-third, and the bottom-third of the existing and the redesigned buildings subjected to 3-component ground motion from the simulated San Andreas fault earthquake.

Maps of the peak interstory drift that occurs in the top-third, middle-third, and bottom-third of the existing and redesigned building models are shown in Figure 6. The redesigned building outperforms the existing building, which reflects the improved design methodology of the UBC97 compared to its 1982 counterpart. The universal localization of damage in the lower floors of both buildings could lead to a greater number of

stories pancaking on top of each other if a single story were to give way, resulting in progressive collapse of the building. Peak interstory drifts in the existing building exceed 0.10 in much of the San Fernando valley, and in many regions of the Los Angeles basin (Santa Monica, West Los Angeles, El Segundo, Compton, Norwalk, Downey, Seal Beach, Fullerton, Santa Ana, Baldwin Park, La Puente, Monrovia, and Alhambra), a value that is indicative of collapse. In Hollywood, Beverly Hills, and downtown Los Angeles, the existing building model experiences peak drifts of 0.04-0.06. The redesigned building model experiences peak drifts of 0.10 or greater in the western half of the San Fernando valley, and peak drifts of 0.06 or greater in the eastern half. Progressing north to south into the Los Angeles basin, the peak drifts in the redesigned building model are in the range of 0.04-0.06. These drifts are indicative of serious damage, warranting building closures and business interruption.

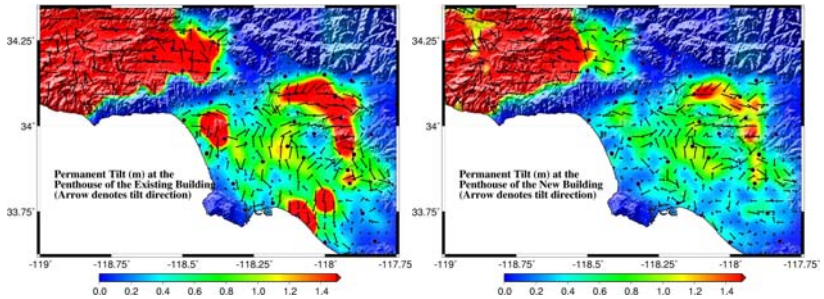

Figure 7: Permanent offset at the penthouse level in the existing and redesigned buildings under the simulated San Andreas fault earthquake. The arrows indicate the tilt magnitude and direction. The scale is saturated at 1.5m, which corresponds roughly to an average inclination of 2% over the building height of the buildings.

Plotted in Figure 7 are the magnitude and direction of the permanent tilt of the existing and redesigned building models, following the earthquake. A six-inch tilt in the Woodland Hills building following the Northridge earthquake led to misalignment in the elevators, resulting in closure and significant direct and indirect costs. The permanent tilts under the 1857-like event are an order of magnitude larger at some locations.

4. BUILDING LOSS ANALYSIS (Muto et al. 2008)

4.1. Basis for Loss Estimation

The cost of replacing the existing or redesigned buildings, $C_{replace}$, with a current state-of-the-art structure is estimated to be approximately $72 M (U.S.), including the cost of structural and non-structural components, and plumbing, electrical, and heating, ventilation & air-conditioning (HVAC) systems; the latter costs are based on estimates for current construction, as shown in the first part of Table 1. The mean loss for the two buildings in this scenario earthquake at each of the 636 analysis sites is computed as the weighted average, $[P*C_{replace} + (1-P)*C_{repair}]$, of the costs associated with two damage states – an irreparable damage state requiring building replacement, with probability P (given the governing EDP), and a reparable damage state with probability (1-P). In this study, it is assumed that "irreparability" of a tall building is dictated solely by the peak residual interstory drift ratio (IDR). The probability of irreparable damage is described using a lognormal cumulative distribution function (CDF) parameterized with logarithmic median peak residual IDR of μ=0.02, and logarithmic standard deviation of β=0.5. For each analysis site, $C_{replace}$ is computed for the two buildings based on this CDF. C_{repair} is computed using the Matlab Damage and Loss Analysis (MDLA, Mitrani-Reiser 2007) toolbox, developed at Caltech to implement the PEER loss-estimation methodology using an assembly-based vulnerability approach (Porter 2000). The toolbox includes damage prediction and repair cost estimation for structural and non-structural components and allows for the computation of the mean and variance of building repair costs conditional on engineering demand parameters (i.e. inter-story drift ratios and peak floor accelerations). Here, it is modified to take into account the special mechanical, electrical and plumbing (MEP) systems utilized in steel-frame high-rises, in addition to the vertical transportation system consisting of high-speed traction elevators.

Probabilistic descriptions of damage to the interior partitions, exterior glazing, acoustical ceiling, and sprinkler system are calculated using fragility functions developed by Porter (2000) that have the form of lognormal CDFs. The governing EDP and fragility function parameters are summarized in the second part of Table 1. While the location and number of connection fractures in the existing building are known from the finite element analysis, a lognormal CDF that is dependent on the peak IDR is assumed for the redesigned building, modeled with ductile connections. Based on observed traction elevator performance in a damaged highrise building during the Northridge earthquake, a fragility function described by a lognormal CDF on peak residual IDR with μ=0.01 and β=0.25 is assumed. The plumbing, electrical, and HVAC systems are assumed to be robust, since serious damage to these components would likely be associated with irreparable structural damage, in which case the entire building must be replaced anyway. Repair and replacement costs for each component are also shown in Table 1. Average repair costs for the fractured moment connections in the existing building are based on a collection of reported values for repairs to fractured connections in steel moment-frame buildings following the 1994 Northridge earthquake (Bonowitz and Maison 2003). Since a major portion of the cost is related to accessing the connection, which will be necessary for both fracture and local flange buckling, the cost for repair for both modes of failure is taken to be the same. Repair and replacement costs for the interior partitions, interior paint, exterior glazing, acoustical ceiling tiles, and sprinklers are given by Porter (2000).

Table 1. Repair/Replacement costs and fragility functions for building components.

Assembly	unit	Quantity	EDP	Fragility Parameters		Action	Cost
				μ	β		($ U.S.)
Structure in irreparable state							
Structure and cladding	ft^2	280,988	Perm. IDR	0.02	0.5	Replace	120
Plumbing systems	ft^2	280,988	Perm. IDR	0.02	0.5	Replace	5
Electrical systems	ft^2	280,988	Perm. IDR	0.02	0.5	Replace	10
HVAC	ft^2	280,988	Perm. IDR	0.02	0.5	Replace	20
Elevators	ea	3	Perm. IDR	0.02	0.5	Replace	1,000,000
Non-structural elements	ft^2	280,988	Perm. IDR	0.02	0.5	Replace	50
Construction costs	ft^2	280,988	Perm. IDR	0.02	0.5	Replace	40
Total cost							71,840,000
Structure in a reparable damage state							
Moment conn. (Bldg. 1; fracture mode)	ea	284	Damage calculated in FEA			Repair	20,000
Moment conn. (Bldg. 2; flange buckling)	ea	550	IDR	0.05	0.5	Repair	20,000
Drywall partitions (visible damage)	64 ft^2	6,098	IDR	0.0039	0.17	Repair	88
Drywall partitions (significant damage)	64 ft^2	6,098	IDR	0.0085	0.23	Repair	525
Drywall finish (visible damage)	64 ft^2	6,098	IDR	0.0039	0.17	Repair	88
Drywall finish (significant damage)	64 ft^2	6,098	IDR	0.0085	0.23	Repair	253
Exterior glazing	panel	3,423	IDR	0.040	0.36	Repair	439
Elevators	ea	3	Perm. IDR	0.01	0.25	Replace	1,000,000
Automatic sprinklers	12 ft	2,757	Accel.	32	1.4	Repair	900
Acoustical ceiling	ft^2	280,988	Accel.	92/(1+w)	0.81	Repair	2.21
Interior paint	ft^2	280,988	Based on ratio of dmg. to undmg. area			Repair	1.52

Table 1: Repair/replacement costs and fragility functions for building components.

5. ESTIMATION OF REPAIR/REPLACEMENT COSTS FOR THE TWO BUILDINGS UNDER THE SCENARIO EARTHQUAKE

The geographical distribution of mean (expected) losses for the two buildings is shown in Figure 8. The existing building performs poorly, with complete losses for locations throughout the San Fernando valley and much of the Los Angeles basin. The performance of the redesigned building is much better; the predicted impact of the scenario earthquake in the Los Angeles basin is considerably lower than for the existing building, though significant losses are predicted in some areas of the San Fernando valley.

Figure 9 shows the losses plotted against the residual peak IDR and the transient peak IDR for all 636 analysis sites. It is clear that at higher excitation levels, losses are dominated by the probability of irreparable damage. For the existing building, 309 of the 636 analysis sites have a greater than 50% chance of irreparable damage, while 176 sites for the redesigned building fall into that category. We see that for a peak transient of IDR of 0.05, the FEMA acceptance criterion for the collapse prevention (CP) performance level, building losses exceed 50% for much of the region, with near-total losses occurring

when the peak IDR exceeds 0.075.

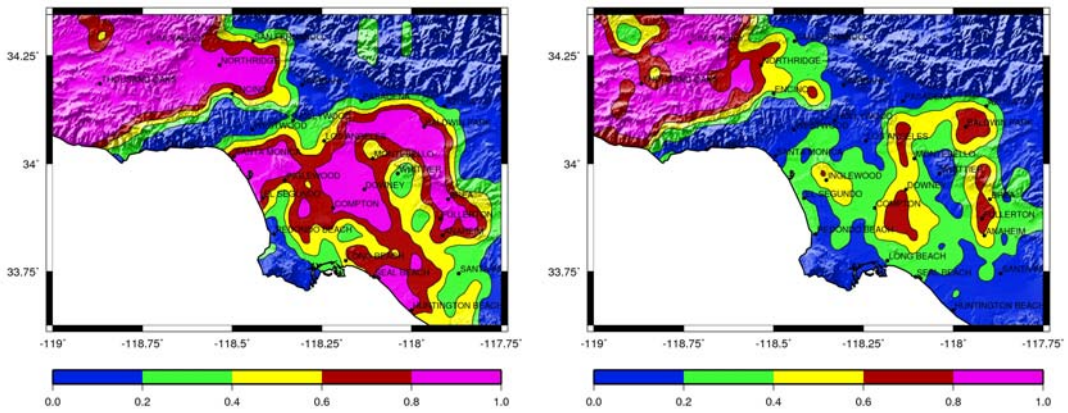

Figure 8: Mean loss for the existing and redesigned buildings normalized by the replacement cost of about $72M. Near-total losses are calculated for the existing building when located in San Fernando valley and much of the Los Angeles basin. Losses for the redesigned building are significantly lower in the Los Angeles basin, but remain high in the San Fernando valley.

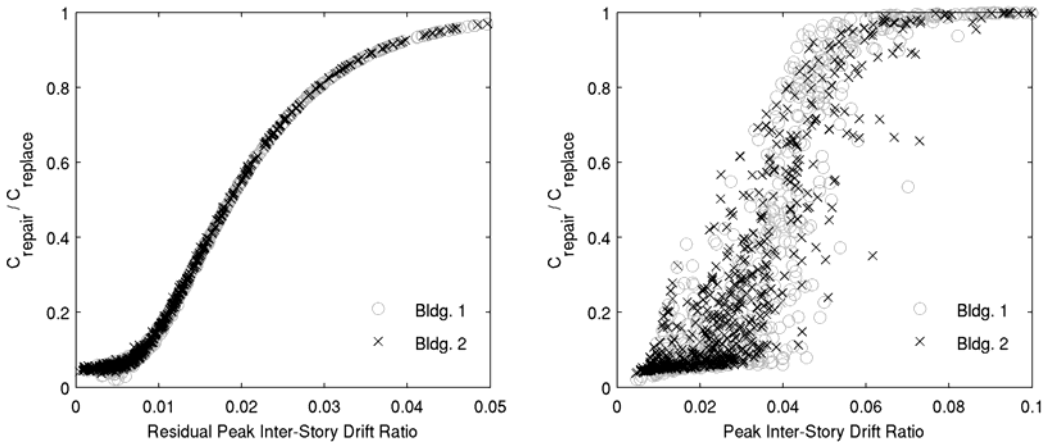

Figure 9: Normalized mean losses for the two buildings plotted against the residual peak IDR and the peak IDR. For values greater than about 0.05, cost is dominated by the probability of irreparable damage. Mean loss for both buildings reaches the replacement cost for peak IDR greater than about 0.075.

6. CONCLUSIONS

In this prototype study, we have laid the framework for performing a quantitative seismic hazard analysis by detailed simulations at all stages: source rupture, seismic wave propagation, structural response, and induced economic loss. The framework allows for effects such as source rupture directivity and slip distribution, both of which play a critical role in determining the intensity of ground motion at a particular site, to be considered. By simulating a large number of plausible earthquakes of varying magnitude from the relevant regional faults and weighing them by their probability of occurrence over a specified time period, it will be possible to develop a more accurate picture of the economic seismic risk faced by a given building. Additionally, by developing a realistic inventory of buildings and other engineered structures, this method can be applied to combine advanced earthquake simulations with structural modeling and PBEE loss methodologies to estimate region-wide losses for major scenario events, which would be very useful in recovery planning.

REFERENCES

Agnew, D. C. and Sieh, K. (1978). A documentary study of the felt effects of the great California earthquake of 1857. *Bulletin of the Seismological Society of America* **68:6**, 1717-1729.

Bonowitz and Maison (2003). Northridge welded steel moment-frame damage data and its use for rapid loss estimation. *Earthquake Spectra* **19:3**, 335-364.

Eguchi, R. T., Goltz, J. D., Taylor, C. E., Chang S. E., Flores, P. J., Johnson, L. A., Seligson, H. A. and Blais, N. C. (1998). Direct economic losses in the Northridge earthquake: A three-year post-event perspective. *Earthquake Spectra* **14:2**, 245-264.

EQE (1995). The Northridge earthquake of January 17, 1994: Report of data collection and analysis, Part A: Damage and inventory data. Tech. Rep. **EQE 36386.02**, EQE International Inc. and the geographic information systems group of the Governor's Office of Emergency Services, California, USA.

Komatitsch, D. and Tromp, J. (1999). Introduction to the spectral element method for three-dimensional seismic wave propagation. *Geophysics Journal International* **139**, 806-822.

Komatitsch, D., Liu, Q., Tromp J., Suss, P., Stidham C. and Shaw J. H. (2004). Simulations of ground motion in the Los Angeles basin based upon the spectral element method. *Bulletin of the Seismological Society of America* **94**, 187-206.

Krishnan, S. and Hall, J. F. (2006a). Modeling steel frame buildings in three dimensions - Part I: Panel zone and plastic hinge beam elements. *Journal of Engineering Mechanics* **132:4**, 345-358.

Krishnan, S. and Hall, J. F. (2006b). Modeling steel frame buildings in three dimensions - Part II: Elastofiber beam element and examples. *Journal of Engineering Mechanics* **132:4**, 359-374.

Krishnan, S., Ji, C., Komatitsch, D. and Tromp, J. (2006a). Performance of two 18-story steel moment frame buildings in southern California during two large simulated San Andreas earthquakes. *Earthquake Spectra* **22:4**, 1035-1061.

Krishnan, S., Ji, C., Komatitsch, D. and Tromp, J. (2006b). Case studies of damage to tall steel moment frame buildings in southern California during large San Andreas earthquakes. *Bulletin of the Seismological Society of America* **96:4**, 1523-1537.

Liu, Q., Polet, J., Komatitsch, D. and Tromp, J. (2004). Spectral-element moment tensor inversions for earthquakes in southern California. *Bulletin of the Seismological Society of America* **94:5**, 1748-1761.

Meltzner, A. J. and Wald, D. J. (1998). Foreshocks and aftershocks of the great 1857 California earthquake. **USGS Open-File Report 98-465**, United States Geological Survey, Pasadena, California, USA.

Mitrani-Reiser, J. (2007). An ounce of prevention: Probabilistic loss estimation for performance-based earthquake engineering. Tech. Rep. **EERL 2007-01**, Earthquake Engineering Research Laboratory, California Institute of Technology, Pasadena, California, USA.

Muto, M., Krishnan, S., Beck, J. L. and Mitrani-Reiser, J. (2008). Seismic Loss Estimation Based on End-to-End Simulation. Proceedings of the first international symposium on life-cycle civil engineering, Varenna, Lake Como, Italy.

Petak, W. J. and Elahi, S. (2000). The Northridge earthquake, USA, and its economic and social impact. Euro conference on global change and catastrophe risk management, Earthquake risks in Europe, IIASA,

Laxenburg, Austria.

Porter, K. (2000). Assembly-based vulnerability of buildings and its uses in seismic performance evaluation and risk-management decision-making. Ph. D. thesis, Stanford University, Stanford, California, USA.

SAC (1995a). Analytical and field investigations of buildings affected by the Northridge earthquake of January 17, 1994 - Part 1. Tech. Rep. **SAC 95-04, Part 1**, Structural Engineers Association of California, Applied Technology Council, and California Universities for Research in Earthquake Engineering, USA.

SAC (1995b). Analytical and field investigations of buildings affected by the Northridge earthquake of January 17, 1994 - Part 2. Tech. Rep. **SAC 95-04, Part 2**, Structural Engineers Association of California, Applied Technology Council, and California Universities for Research in Earthquake Engineering, USA.

SAC (1995c). Surveys and assessments of damage to buildings affected by the Northridge earthquake of January 17, 1994. Tech. Rep. **SAC 95-06**, Structural Engineers Association of California, Applied Technology Council, and California Universities for Research in Earthquake Engineering, USA.

Shaw, J. H. and Suppe, J. (1996). Earthquake hazards of active blind-thrust faults under the central Los Angeles basin. *Journal of Geophysical Research* **101:B4**, 8623-8642.

Sieh, K. E. (1977). Slip along the San Andreas fault associated with the great 1857 earthquake. *Bulletin of the Seismological Society of America* **68:5**, 1421-1448.

Sieh, K. E. (1978). Pre-historic large earthquakes produced by slip on the San Andreas fault at Pallett Creek, California. *Journal of Geophysical Research* **83**, 3907-3939.

Suss and Shaw (2003). P-wave seismic velocity structure derived from sonic logs and industry reflection data in the Los Angeles basin. *Journal of Geophysical Research* **108:B3**, Article no. 2170.

Weldon, R. J., Fumal, T. E., Biassi, G. P. and Scharer, K. M. (2005). Past and future earthquakes on the San Andreas fault. *Science* **308**, 966-967.